

RESEARCH ARTICLE | SEPTEMBER 03 2024

A versatile system for the growth of porphyrin films via electro spray and molecular sublimation in vacuum and their multi-technique characterization

F. Goto ; A. Calloni  ; R. Yivlialin ; A. Bossi ; F. Ciccacci ; L. Duò ; J. N. O'Shea ; G. Bussetti 



Rev. Sci. Instrum. 95, 095102 (2024)

<https://doi.org/10.1063/5.0223459>



Articles You May Be Interested In

X-ray absorption and photoemission spectroscopy of zinc protoporphyrin adsorbed on rutile TiO₂ (110) prepared by *in situ* electro spray deposition

J. Chem. Phys. (February 2010)

Dual-axis thrust stand for the direct characterization of electro spray performance

Rev. Sci. Instrum. (June 2022)

Mask-less patterning of organic light emitting diodes using electro spray and selective biasing on pixel electrodes

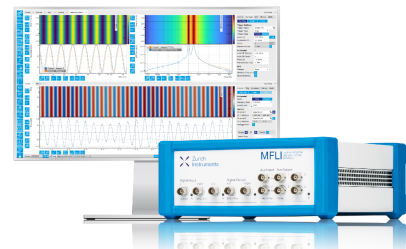
Appl. Phys. Lett. (April 2015)

Challenge us.

What are your needs for periodic signal detection?



Find out more



A versatile system for the growth of porphyrin films via electrospray and molecular sublimation in vacuum and their multi-technique characterization

Cite as: Rev. Sci. Instrum. 95, 095102 (2024); doi: 10.1063/5.0223459

Submitted: 14 June 2024 • Accepted: 9 August 2024 •

Published Online: 3 September 2024



View Online



Export Citation



CrossMark

F. Goto,¹ A. Calloni,^{1,a)} R. Yivlialin,¹ A. Bossi,² F. Ciccacci,¹ L. Duò,¹ J. N. O'Shea,³
and G. Bussetti¹

AFFILIATIONS

¹ Department of Physics, Politecnico di Milano, Piazza Leonardo da Vinci 32, I-20133 Milano, Italy

² Istituto di Scienze e Tecnologie Chimiche "G. Natta" del Consiglio Nazionale delle Ricerche (CNR-SCITEC), via Golgi 19, I-20133 Milano, PST via G. Fantoli 16/15, Milano I-20138, Italy

³ School of Physics and Astronomy, University of Nottingham, University Park, Nottingham NG7 2RD, United Kingdom

^{a)} Author to whom correspondence should be addressed: alberto.calloni@polimi.it

ABSTRACT

We present a system for the growth of molecular films in vacuum that exhibits high versatility with respect to the choice of molecular species. These can be either evaporated from powders or injected from solutions using an electrospray system, making it possible to handle particularly large and/or fragile molecules in a controlled environment. The apparatus is equipped with a reflectance anisotropy spectroscopy system for the *in situ* characterization of the optical response of the films and can be directly connected to a photoelectron spectrometer without breaking the vacuum. The system is conceived for the study and characterization of porphyrin films. Here, to showcase the range of possible analyses allowed by the experimental setup and test the operation of the system, novel results are provided on electrospray deposition on highly oriented pyrolytic graphite of Zn tetraphenyl porphyrins and Zn proto porphyrins, the latter featuring fragile side groups that make deposition from solution more attractive. *In situ* characterization is complemented by *ex situ* atomic force microscopy. Thanks to this multi-technique approach, changes in the film morphology and spectroscopic response are detected and directly related to the choice of the molecular moiety and growth method.

© 2024 Author(s). All article content, except where otherwise noted, is licensed under a Creative Commons Attribution-NonCommercial-NoDerivs 4.0 International (CC BY-NC-ND) license (<https://creativecommons.org/licenses/by-nc-nd/4.0/>). <https://doi.org/10.1063/5.0223459>

I. INTRODUCTION

Porphyrin molecules, involved in natural processes such as oxygen capture in blood and light harvesting in plant tissues, have found a number of technological applications such as protective coatings,^{1–3} active elements in gas sensors,^{4–6} optoelectronic devices and solar cells,^{7–9} or in perspective molecular electronic devices.^{10,11} Their ubiquitous use stems from their particular ring-like shape and the possibility of hosting a metallic ion at their center, which maximizes and allows the tuning of molecular interactions with the environment. The molecular periphery can also be decorated with a variety of side groups that affect, for instance, molecular solubility and intermolecular interactions, leading to a range of assemblies

and morphologies.^{12–14} The interaction of porphyrins with surfaces gives rise to a complex phenomenology, including specific chemical or electronic effects,^{15–17} and often results in highly ordered self-assembled molecular structures.^{18,19} Therefore, from a technological standpoint and to improve our fundamental understanding of porphyrin physicochemical behavior, a high degree of control over the growth of thin and ultra-thin porphyrin films is required in terms of their purity and morphology. It is also of paramount importance to preserve the integrity of the molecular species, especially when they are either very large or feature labile side groups.

In contrast to common deposition methods, such as the casting of molecules on a substrate from solution (drop casting, spin coating, etc.), molecular evaporation in vacuum usually results in very

uniform layers, free from contaminants/solvent inclusions. In addition, by monitoring the fluxes of evaporated species, it is possible to attain a high degree of control over the stoichiometry of the molecular blends and multilayer structures.^{20–22} Molecular evaporation, however, is not always applicable. Although the porphyrin core is usually very resistant upon sublimation, requiring high temperatures on the order of 600 K, some specific formulations may undergo fragmentation via the removal of the molecule's peripheral groups, or scission in the case of large porphyrin-containing molecular aggregates.^{23–25}

To overcome these limitations, electrospray deposition (ESD) was introduced, a technique that relies on the direct extraction of molecular species from solution, aided by an electric field.²⁶ The solution is passed through a high voltage needle (called the emitter) facing a grounded counter electrode. Under certain working conditions, a conical (the so called Taylor cone) stream of liquid is extracted from the emitter and breaks into charged droplets, accelerated by the field. As a result of electrostatic interactions and the continuous evaporation of the solvent, droplets undergo fissions and spread laterally, thus forming a “plume” hitting the substrate. This technique has been further modified to collect the droplets by means of a capillary and send them to the substrate in a vacuum environment.²⁶ This approach has several advantages: (i) vacuum aids in the removal of the solvent from the droplets, ideally forming a pure molecular flux; (ii) the substrate can be prepared in vacuum and preserved from reactive gases present in the ambient atmosphere or from airborne contaminants; (iii) flying particles are charged and therefore can be collected by proper electrostatic optics and filtered depending, for example, on their mass, before reaching the substrate.

ESD in vacuum has been employed for the controlled growth of a number of molecular species—including porphyrins—such as molecular nano rings,²⁷ single molecule magnets, and dye molecules.^{28,29} In the following, we present a versatile experimental setup for the growth and *in situ* characterization of thin and ultra-thin porphyrin layers in a controlled environment, equipped with an organic growth chamber with both standard effusion cells for molecular sublimation and an ESD system. The optical response of the molecular films can be monitored during their growth by Reflectance Anisotropy Spectroscopy (RAS), a technique originally developed for the *in situ* characterization of semiconductor surfaces and epitaxial semiconductor growth,^{30–32} and later applied to hybrid (organic/inorganic) systems.^{33,34} In our setup, RAS spectra can be acquired simultaneously with molecular evaporation and quasi-simultaneously with ESD by temporarily tilting the sample away from the flux of sprayed molecules. The growth chamber is also connected to a larger vacuum system composed of (i) a preparation chamber for substrate conditioning and the growth of inorganic (metal or oxide) films and (ii) a spectroscopy chamber housing an electron spectrometer, thus allowing for the investigation of sample composition and electronic properties by means of X-ray and UV photoelectron spectroscopy (XPS and UPS, respectively). The resulting experimental setup provides a large degree of flexibility in terms of molecule/substrate combinations and a high degree of control over the growth conditions, in line with other recent efforts toward the in-vacuum realization of tailored organic interfaces and multilayer hybrid systems.^{35,36}

The performance of the experimental apparatus is investigated by growing films of two porphyrin moieties, namely, Zn tetraphenyl

porphyrins (ZnTPP) and Zn protoporphyrins (ZnPP). Here, ZnPP is considered a prototypical molecule with fragile side groups (see below), for which ESD in vacuum is preferred (see, e.g., Ref. 37), although careful evaporation (i.e., at very low rates) of protoporphyrins has also been reported.³⁸ The same ESD parameters are applied to ZnTPP ESD to investigate the effect of a change in the periphery of the molecules on the film characteristics. Rather thick films have been grown on a relatively inert substrate such as Highly Oriented Pyrolytic Graphite (HOPG) to (i) provide strong spectroscopic signatures and (ii) allow for a complementary *ex situ* investigation with Atomic Force Microscopy (AFM). In addition, ZnTPP films on HOPG obtained by vacuum evaporation are used as a reference, given the large amount of information present in the literature, including the authors' previous studies,³⁹ to ease the interpretation of these first ESD results obtained with the presented setup.

A. The experimental apparatus

Figure 1 is a schematic representation of the experimental apparatus engineered by the authors. The overall setup was designed to provide a controlled environment for the spectroscopic investigation of a variety of different systems, either brought from outside or produced *in situ*. Typical substrates are crystalline metals, semiconductors, or graphite, as in the present case. A range of materials can be grown in the form of thin and ultra-thin films, from epitaxial metallic layers to metal oxides and organic films. In this respect, the new organic growth chamber significantly enhances the versatility of the system by increasing the number of candidates for organic film production with non-evaporable molecules. The available analytical techniques allow for a complete characterization of the electronic structure of samples, from core orbitals to valence states (both filled and empty), with spin resolution⁴⁰ of interest for the detection of magnetic effects in molecular films.¹⁷ Optical spectroscopy can be performed in the new organic growth chamber, whereas for

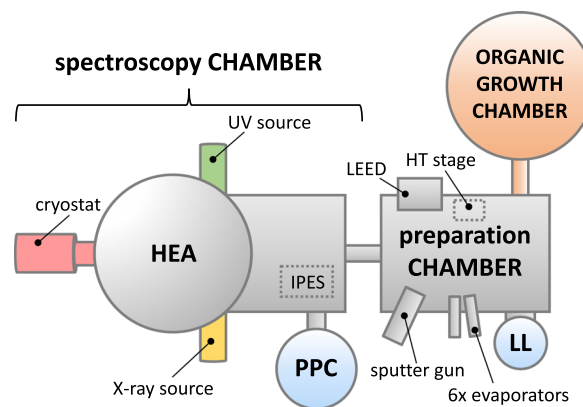


FIG. 1. Experimental apparatus for the growth and *in situ* characterization of organic (namely, porphyrin) films. Molecular evaporators, the electrospray deposition system, and the setup for optical spectroscopy are housed in the “organic growth chamber” (described with details in the main text). Substrate preparation takes place in the “preparation chamber,” while the necessary tools for electron spectroscopy (the hemispherical electron analyzer, HEA, x-ray and UV sources, and the apparatus for inverse photoemission spectroscopy, IPES) are installed in the “spectroscopy chamber.” “PPC” is the chamber for IPES photocathode preparation, while “LL” is the load lock chamber.

microscopic characterization, samples can be transferred outside the apparatus in a protected atmosphere by passing through a load lock (LL in Fig. 1).

The preparation and spectroscopy chambers are operated at a base pressure in the high 10^{-11} mbar range; the preparation chamber is equipped with an Ar^+ sputter gun from Physical Electronics Inc. The beam of accelerated Ar^+ ions (up to a kinetic energy of 4 keV) can be raster-scanned over an area of approximately one square centimeter. Sample annealing can be performed on a home-made molybdenum heating stage, up to a maximum temperature of 2300 K, checked by means of an optical pyrometer. A rear-view low energy electron diffraction (LEED) instrument from Physical Electronics Inc. is available to check the surface quality of crystalline substrates. In addition, the preparation chamber is equipped with a home-made water cooled evaporation cluster for the growth of metallic films, consisting of e-beam evaporators and crucibles for use with low melting point metals. Pure gases can be dosed by using leak valves. The spectroscopy chamber is equipped with a 150 mm hemispherical electron analyzer (HEA) from Specs GmbH, coupled with a multichannel detector and a Mott detector for spin resolved studies.⁴⁰ UV photons are provided by a duoplasmatron source (UVS300 from Specs) that can be operated with He gas, producing HeI and HeII radiation at 21.2 and 40.8 eV, respectively. A dual anode source is used to produce Mg and Al K α photons at 1253.6 and 1486.6 eV, respectively, for XPS. Inverse photoemission spectroscopy (IPES) is used for the characterization of empty electronic states and is based on the detection of UV radiation coming from the de-excitation of low energy electrons produced by an electron gun.⁴¹ Electrons are generated by the light excitation of a GaAs crystal, previously prepared in the photocathode preparation chamber (PPC in Fig. 1).⁴² The spectroscopy chamber is equipped with a four-axis manipulator working at variable temperatures, from room temperature (RT) down to about 30 K, thanks to a closed-cycle He cryostat.

B. The organic growth chamber

The organic growth chamber, operated at a base pressure in the low 10^{-9} mbar range, is equipped with standard facilities for molecular evaporation, including (i) four individually shuttered effusion sources and (ii) a water-cooled quartz microbalance to assess the evaporation rate. During molecular evaporation, the sample can be optionally transferred from the manipulator to a small stage equipped with a resistive heater and a reservoir for liquid nitrogen to vary its temperature from 160 K up to about 400 K. The ESD system from MolecularSpray Ltd. (model UHV4i) is connected by means of a vacuum valve, as schematically shown in Fig. 2(a). In the same figure, the RAS apparatus is also reproduced [Fig. 2(b)]. To perform the optical characterization, a collimated light beam (represented by a red line) is sent on the sample at near normal incidence, and the reflected beam is collected through the same viewport, placed at the bottom of the growth chamber.

1. The effusion sources

The effusion sources are mounted at the bottom of the organic growth chamber, tilted by 15° with respect to the chamber's axis. The distance between the opening of the crucible and the sample surface is about 15 cm. The effusion sources, schematically represented in Fig. 2(c), were designed and produced by Cinquepascal S.r.l. Molecular powders are inserted in a quartz crucible (internal volume of 0.6 cm^3 , 2.5 cm in length) heated by a Ta foil up to a maximum temperature of 900°C . Thermal insulation is provided by a boron nitride (BN) enclosure. The crucible temperature, measured by means of a type K thermocouple, is kept at the evaporation setpoint (within 0.1°C) by means of a Proportional-Integral-Derivative (PID) regulator.

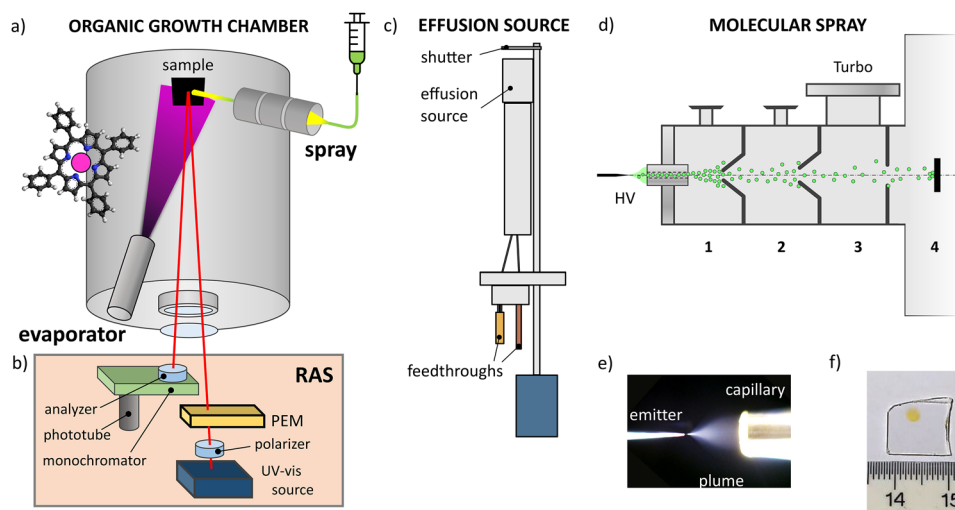


FIG. 2. Overview of the experimental setup: (a) chamber for porphyrin films growth housing an effusion cell, the electro spray deposition (ESD) system, and (b) the reflectance anisotropy spectroscopy (RAS) apparatus; (c) schematics of the effusion source; (d) schematics of the electro spray setup; (e) picture of the emitter region during the spray; (f) molecular film (the yellow circle about 2 mm wide) deposited on a glass slide.

2. The electrospray deposition system

A schematic layout of the various parts of the ESD system is presented in Fig. 2(d). As already discussed, ESD is based on the ionization of a solution containing the molecules by passing it through a thin emitter (a small silica tube with an internal diameter of 100 μm), kept at a high voltage (between 1.5 and 3 kV). A syringe pump is used to feed the solution into the emitter at a fixed flow rate (in the ml/h range). The emitter faces a larger steel capillary, placed at a distance of about 8 mm, which directly injects the liquid into the vacuum system through a narrow passage (50 mm in length and 250 μm in diameter).⁴³ The emitter is placed on a five-axis micrometric stage, and a macro camera overlooks the spray region for precise alignment. The “spray plume” is shown in Fig. 2(e). The entrance capillary is placed at the first stage of a differentially pumped conduit, composed of three stages (operating at decreasing pressure: ~ 1 , 10^{-1} , and 10^{-4} mbar, respectively). At present, the carrier gas for the solution droplets and molecular ions is ambient air at atmospheric pressure. Skimmers (i.e., conical apertures) with internal diameters of 0.4 and 0.6 mm, respectively, are used to minimize the perturbation on air flow in stages 1 and 2. In stage 3, molecular flow prevails, and a simpler circular orifice (1.0 mm internal diameter) is interposed with the growth chamber. In our system, the sample is placed about 20 cm away from the last exit aperture. The first two stages are connected to two independent 150 l/min rotary pumps, while the third stage is directly connected to a 70 l/s small turbo pump backed by the second stage rotary pump. The growth chamber is pumped using a 260 l/s turbopump. Under operating conditions (ESD system connected), the pressure in the growth chamber remains in the low 10^{-7} mbar range, where the pressure increase is due to air molecules leaking through the ESD apertures. The pressure increases to a high 10^{-7} mbar, mainly related to the presence of solvent molecules, upon switching on the high voltage, thereby accelerating the solution toward the vacuum system. The ESD system has been engineered with ease of use and mounting flexibility in mind. The substrate is in direct line of sight of the emitter, and no electrostatic lenses are used to filter out ionized porphyrin molecules from the main stream of particles. Therefore, no direct control over the energy of the incoming molecules or the actual composition of the sprayed beam is possible.⁴⁴ The implementation of more complex devices to characterize and potentially filter the ESD beam, such as a mass spectrometer, is in general possible, as shown in Ref. 45, but it would be a rather bulky and complex extension to the described experimental apparatus.

The landing point of the molecules on the sample can be determined by placing a small laser diode in the emitter position and focusing the light beam at the capillary entrance. The laser test is also useful for checking the alignment of the ESD system apertures upon assembling the pumping stages and to detect possible clogging along the molecular path. Fluorescein dye molecules ($\text{C}_{20}\text{H}_{12}\text{O}_5$), dissolved in a 1 mM 50:50 solution of water and ethanol, were deposited on a glass slide to determine the extension of the sprayed area on the sample. The deposition resulted in a nearly circular spot ~ 2 mm in diameter [Fig. 2(f)]. The ESD system is monitored throughout the molecular deposition process: small corrections to the emitter position/voltage and to the flow rate have to be applied to maintain the chamber pressure at a nearly constant value, indicative of the unobstructed flow of solvent molecules throughout the spray system.

3. The reflectance anisotropy spectroscopy system

RAS experiments are performed using the custom-made setup schematized in Fig. 2(b) (more details in Ref. 46). It is composed of a Xe arc lamp that sends a collimated beam of light through a linear polarizer, followed by a photoelastic modulator, which switches the light polarization along two orthogonal directions (α and β) at a frequency of 100 kHz. The emerging light is focused on the sample (within a spot of ~ 2 mm radius), and the reflected beam then passes through a second linear polarizer and enters a monochromator coupled to a photomultiplier. The anisotropy signal is defined as the normalized difference between the reflected light intensities for the two beam polarizations:

$$\frac{\Delta R}{R} = 2 \frac{R_\alpha - R_\beta}{R_\alpha + R_\beta}.$$

The intensity is maximized by aligning the RAS optical axes to specific anisotropy directions of the sample under investigation, as thoroughly discussed in the next section. As already mentioned, to send light through the same viewport, the incident and reflected beams are nearly collinear and therefore should impinge normally on the sample surface. In the present experimental configuration shown in Fig. 2(a), RAS and molecular evaporation can be performed simultaneously, whereas a 90° sample rotation is necessary to perform ESD. The acquisition of a RAS spectrum in the 2–3.5 eV photon energy range (encompassing the main features related to visible-light adsorption from porphyrin molecules) requires a few minutes, during which the substrate is removed from the stream of sprayed molecules.

II. PORPHYRIN FILMS GROWTH AND CHARACTERIZATION

Figure 3 shows the chemical structures of (a) Zn tetraphenyl porphyrin (ZnTPP) and (b) Zn protoporphyrin (ZnPP). The porphyrin ring is composed of four pyrrole aromatic groups (hence the name macro-cycle) connected by methine bridges. The N atoms of the pyrrole groups hold in position a Zn^{II} ion. The resulting structure is responsible for the overall chemical and optical activity of porphyrins because the frontier electronic orbitals (highest occupied and lowest unoccupied molecular orbitals, HOMO and LUMO, respectively) are localized there. The perimeter of the porphyrin molecule is decorated by (a) four pyrrole groups attached in *meso*

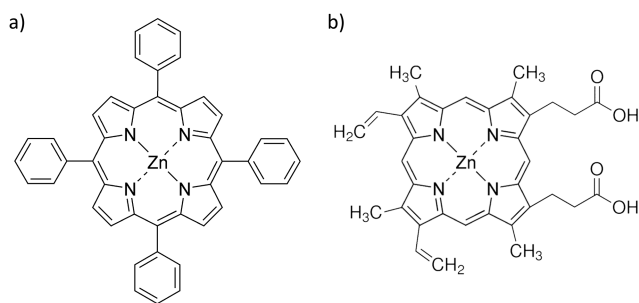


FIG. 3. Chemical structure of (a) Zn tetraphenyl porphyrin and (b) Zn protoporphyrin.

positions (hence, the name Zn tetraphenyl porphyrin) or (b) four methyl groups, two vinyl groups, and two carboxylic groups, all in β positions, that is, directly attached to pyrroles. The latter molecule is the result of the coordination of a Zn ion with protoporphyrin IX, a precursor (hence the term “proto”) to many biological compounds such as heme or chlorophyll.⁴⁷

A. Experimental details

HOPG crystals ($10 \times 10 \text{ mm}^2$ wide, Z grade, purchased from Optigraph GmbH) were exfoliated with an adhesive tape and swiftly inserted into vacuum. ZnTPP and ZnPP were purchased from Merck GmbH. For ESD, molecules were dissolved in a 1:1 methanol:toluene solution at a concentration of 1 mg per 10 ml of solution. Typical deposition parameters (also used for fluorescein deposition) were a flow rate of about 1 ml/h and a deposition time of about 3 h. ZnTPP was also loaded in one of the effusion cells in a quartz crucible and thoroughly degassed before film growth. The evaporation rate was about 0.5 \AA/s .

In situ photoelectron spectroscopy (XPS and UPS) experiments were performed by exciting the molecular films with Mg K α and He I photons, respectively. The pass energy of the hemispherical analyzer was set to 20 and 0.7 eV for XPS and UPS, yielding a Full Width at Half Maximum (FWHM) energy resolution of about 1 eV and 30 meV, respectively.

AFM characterizations were performed *ex situ* with a commercial Keysight 5500 microscope, operated in tapping mode, with silicon tips from Bruker (cantilever force constant 37 N/m; $\nu_0 = 320 \text{ kHz}$) and a scan rate of about 1 Hz.

B. Results and discussion

1. Morphological and optical characterization

The results of the morphological characterization of the molecular films are presented in Figs. 4(a)–4(c). On a millimeter scale, the deposition spot appears to be fairly uniform (see, for instance, the characterization presented in Ref. 48), while a certain variability is observed by investigating different locations across the sprayed area with AFM, particularly with respect to the overall amount of deposited material. Nevertheless, the reported images are representative of the characteristic morphology observed in the samples: sprayed films appear rather rough owing to the presence of irregular porphyrin clusters, with the largest ones (with lateral sizes also exceeding $1 \mu\text{m}$) present on the ZnTPP sample. The above morphologies are contrasted with that observed on the evaporated film [Fig. 4(a)], where the nominal thickness of the molecular layer (about 150 nm) was chosen to approximate the amount of material covering the HOPG surface in the two sprayed samples. The evaporated film shows a strikingly different morphology, characterized by a fine distribution of square islands (of variable lateral scale, from tens to hundreds of nanometers, as observed in the detailed image) roughly oriented along the HOPG steps, still visible in the large scale image. The observed morphology is fully compatible with the results already obtained by the authors for thinner (<10 nm) ZnTPP films (see, for instance, Ref. 49) and is basically driven by molecular adsorption from the gas phase and diffusion on the surface. The islands are crystalline, and molecular packing is likely the one found on macroscopic ZnTPP crystals.⁵⁰ In vacuum

evaporated samples, the size and separation of porphyrin islands are affected by several factors; in general, different porphyrin moieties or growth conditions may give rise to different morphologies.^{39,49} This phenomenology could, in principle, also be observed in sprayed samples; however, other factors have to be taken into account, such as (i) the different physics leading to molecular arrival on the HOPG surface and (ii) the different environmental conditions. While in the case of molecular evaporation, the kinetic energy of the molecules is limited by thermal agitation within the heated crucible, the use of pressure differentials in the ESD setup might lead to molecular acceleration.⁵¹ An increased kinetic energy of the adsorbed porphyrin molecules is expected to retain or even enhance the regularity of the evaporated film.^{52,53} Unfortunately, however, this beneficial effect is not directly evident in the observed sprayed film morphology. In the present case, we rather attribute the irregular structures observed in Figs. 4(b) and 4(c) to the effect of residual solvent evaporation from the surface,⁵⁴ as pointed out in other studies on ESD.^{48,55,56} In this respect, the slightly different morphology observed for ZnTPP and ZnPP might be attributed to the details of the molecule-solvent interaction.⁵⁷ Interestingly, however, large (hundreds of nanometers) and relatively flat aggregates are observed between the ZnTPP clusters [Fig. 4(b), the area highlighted in the inset], possibly directly influenced by the details of the molecule/substrate interactions in close proximity to the interface. The same insight is unfortunately out of reach for the ESD ZnPP film because of the larger density of molecular clusters.

Complementary information on porphyrin organization at the surface is provided by RAS [Fig. 4(d)]. The interpretation of the RAS signal is not straightforward because both isolated molecules and molecular films can exhibit an anisotropic optical response. In the ZnTPP and ZnPP molecules, optical transitions in the UV–vis energy range are localized within the macro-cycle (the Soret band), whose position settles at about 420–430 nm for both ZnTPP and ZnPP in solution,^{58,59} as highlighted by the gray rectangle in Fig. 4(d). ZnTPP molecules are isotropic and, therefore, do not contribute to the RAS signal when they lie flat on the substrate. However, this configuration is lost when molecules crystallize, as in molecular films, because they can exhibit a tilt angle with respect to the buried substrate.⁶⁰ In these films, a preferential anisotropy direction cannot be established *a priori* but must be evaluated experimentally by performing an azimuthal analysis of the RAS signal intensity.⁶¹ We verified that the RAS signal is maximized on HOPG by choosing the α (β) light polarization direction to be parallel (orthogonal) to the direction of HOPG exfoliation, given the observation that this operation is able to preferentially orient the HOPG step edges and, in turn, the porphyrin anisotropy direction.¹⁶ Interestingly, the anisotropy promoted by the HOPG morphology can also be detected in relatively thick films.⁶¹

In Fig. 4(d), the RAS spectrum of the evaporated film shows a feature at about 465 nm. Considering that a shift toward higher wavelengths is expected for ZnTPP molecules in the condensed phase,⁶² this feature corresponds to optical transitions within the Soret band. In the same spectral region, only a faint (around 1%) signal is detected on the ESD ZnTPP layer, which is related to the presence of molecular crystals, as in the case of ZnTPP evaporation [see the inset of Fig. 4(b)]. The ZnPP molecules are expected to contribute to RAS in the investigated spectral region; unfortunately, no signal is detected in the ZnPP samples, suggesting the formation of

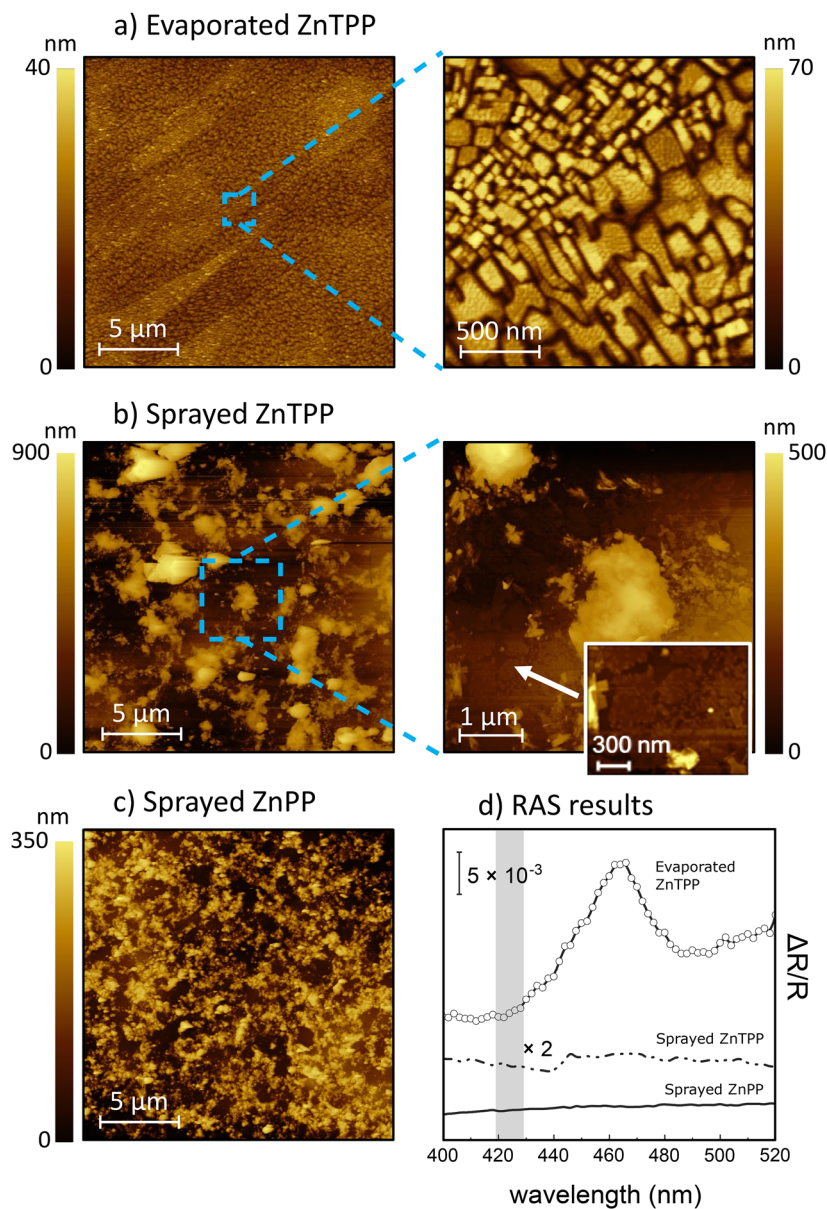


FIG. 4. *Ex situ* atomic force microscopy (AFM) images acquired on a thick ZnTPP layer (a) vacuum evaporated and (b) obtained by ESD on HOPG. The inset highlights an area with a more regular morphology (see the main text). (c) AFM image acquired on a thick ZnPP film obtained by ESD on HOPG. (d) *in situ* RAS results obtained on the above films, the gray region marks the position of ZnTPP and ZnPP Soret band maxima in solution.

an isotropic film. We note that “isotropic” is not only associated with the loss of coherence with the direction of HOPG steps but could also indicate the formation of a disordered or amorphous local molecular structure. Molecular evaporation and ESD can therefore produce thin films with different degrees of optical anisotropy, from highly oriented systems to fully isotropic molecular assemblies. This is possible by exploiting the specific characteristics of the two deposition techniques as well as the chemical tunability of the selected molecular species.

2. Photoelectron spectroscopy characterization

The photoelectron spectroscopy characterization of the ZnTPP and ZnPP sprayed films considered in the previous paragraph is shown in Fig. 5. A comparison is made with a representative ZnTPP sample with a thickness of about 10 nm. Panels (a) and (b) relate to the Zn $2p_{3/2}$ and N $1s$ binding energy (BE) regions, respectively. Starting from the top of the figure, spectroscopic results from the vacuum evaporated ZnTPP film are shown in black, the ESD ZnTPP

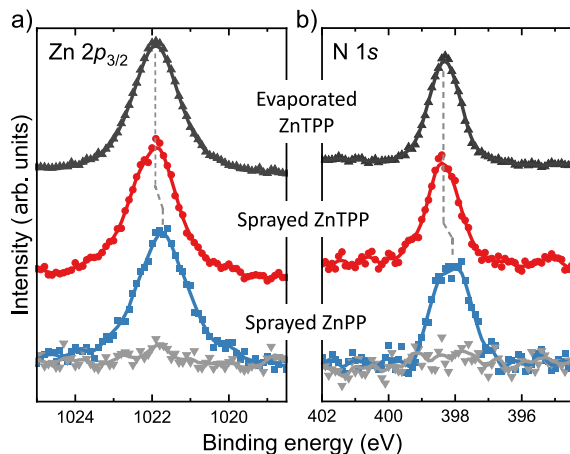


FIG. 5. XPS results related to (a) the Zn $2p_{3/2}$ and (b) the N $1s$ spectral regions, acquired on evaporated and ESD grown ZnTPP samples (black and red symbols, respectively) and on the ESD grown ZnPP sample (blue symbols). The gray spectra are acquired in a HOPG region not covered with molecular species. All spectra are normalized to the N $1s$ peak intensity. Source satellites have been subtracted from the raw spectra, together with a Shirley background.

film in red, and the ESD ZnPP one in blue. All spectra were acquired in magnification mode, that is, by imaging only a portion of the overall HOPG surface, roughly of the same size of the sprayed film. Therefore, in the case of ESD grown samples (the evaporated film covers the totality of the HOPG surface), we were able to characterize the sample surface also outside the area hit by the molecular beam. The latter characterization is shown with gray triangles in Fig. 5: as expected, neither N nor Zn signals are detected. Photoemission from the C $1s$ BE region (not shown) is not considered here, given the large signal coming from the HOPG substrate, even in sprayed areas. The intensity of the spectroscopic features from sprayed films is significantly reduced with respect to the intensity of the related features from the evaporated one. This might be due to the presence of uncovered HOPG areas within the imaged region (provided we had to compromise between spatial resolution and signal intensity during the measurements), but also to the presence of areas covered by a thin molecular film, as suggested by the morphology observed by AFM [Fig. 4(b)], thin enough not to block photoelectrons from the substrate. Given the high surface sensitivity of the photoemission technique (in the nm range), the contribution to the overall photoemission signal expected from thick molecular clusters is nevertheless limited to the topmost molecular layers and therefore scales with the effective surface covered by such aggregates.

Quantitative analysis of the Zn $2p_{3/2}$ and N $1s$ spectra gives an N:Zn ratio of 4:1 ($\pm 20\%$) for all samples, in agreement with the expected stoichiometry of the porphyrin molecules. The positions of the observed spectroscopic features and their mutual BE distance are also in agreement with previous investigations of ZnTPP and ZnPP porphyrins.^{63–66} Interestingly, features related to ZnTPP molecules show nearly the same BE and line shape on both evaporated and sprayed films, while a shift of about 0.2 eV toward lower BE and a slightly broader N $1s$ line shape are observed for the ZnPP sample.

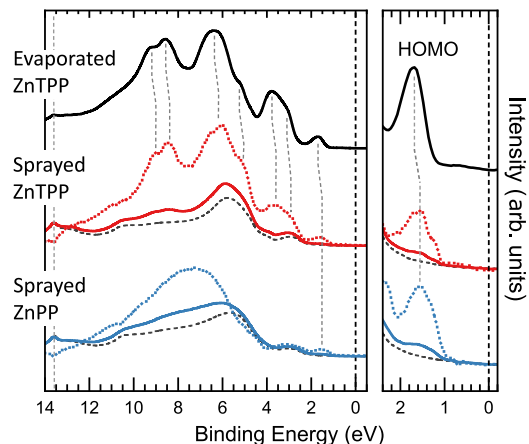


FIG. 6. UPS results acquired on evaporated and ESD grown ZnTPP samples (thick black and red lines, respectively) and on the ESD grown ZnPP sample (thick blue lines). The left panel is a zoom in the [2.4, -0.2] eV range. Representative spectra from the underlying HOPG substrate are reported with black, dotted lines. Dotted red and blue lines are difference spectra (measured spectra—substrate), representative of photoemission from ZnTPP and ZnPP molecules, respectively, normalized to match the peak intensity of the top spectrum (from the evaporated sample). Source satellites have been subtracted from the raw data.

The same samples were analyzed using UPS, and the related spectra are shown in Fig. 6. As in the case of the XPS data, the spectra acquired from the sprayed area (thick lines in Fig. 6) are compared with those representative of the HOPG surface (black dotted lines), retrieved by moving the sample under the UV light beam. This is particularly relevant for the analysis of the valence band structure, where the photoemission signal from the molecular orbitals partially overlaps with that from the HOPG substrate. The latter is characterized by broad features (roughly at 3 and 6 eV due to photoemission from π and σ C sp^2 orbitals⁶⁷), and a characteristic peak at about 13.5 eV due to secondary electrons scattering.⁶⁸ In Fig. 6, the red and blue dotted lines are the result of the subtraction between the signal measured on ESD grown ZnTPP and ZnPP films, respectively, and that on the bare HOPG surface measured on the same sample. No subtraction is needed for the spectrum acquired from the evaporated sample (thick black line), which is representative of photoemission from ZnTPP molecules.^{63,69} If we consider the photoemission signal from molecular species, both ZnTPP samples (the evaporated and the ESD grown ones) show a very similar line shape, featuring a number of photoemission peaks extending up to a BE of about 10 eV, while photoemission from ZnPP molecules is characterized by comparatively fewer features. These differences are related to the presence (absence) of photoemission features from the phenyl groups in ZnTPP (ZnPP), as can be appreciated by comparing the gas phase photoemission results from MTPP and metal octaethylporphyrins (featuring eight ethyl side groups, therefore much similar to MPP).^{70,71} Close to the Fermi energy (E_F), all molecules show characteristic features due to photoemission from the inner molecular ring (Fig. 6, left panel).^{70,72} The feature at about 1.7 eV is related to photoemission from the highest occupied molecular

orbitals (HOMO) and is seen to broaden and shift toward lower BE on ESD samples.

Providing an explanation for the small spectral differences between the evaporated and sprayed films, shown in Figs. 5 and 6, is challenging. Photoemission from ultra-thin porphyrin films is often characterized by broader features and BE shifts, similar to those observed on the sprayed samples. These occurrences result from charge transfer,^{73,74} porphyrin skeleton distortion,^{63,75} or even demetalation,^{37,76} as well as from photoelectron hole screening,^{77,78} all due to the molecular proximity to the substrate. Although thinner porphyrin layers may indeed contribute to the overall photoemission intensity, as also suggested by our morphological characterization, similar spectral modifications are generally reported in thick molecular films depending, for instance, on the band alignment at the interface with the buried substrate⁷⁹ and/or screening effects,⁸⁰ in turn related to molecular packing and crystallographic degree of order.^{80–82} Overall, the photoemission data confirm the formation of stoichiometric ZnTPP and ZnPP molecular layers, where molecules largely retain their characteristic electronic structure, with some differences related to the details of molecule/molecule and molecule/substrate interaction, whose investigation is beyond the scope of the present work.

III. CONCLUSIONS

We successfully commissioned and operated a versatile apparatus featuring electrospray deposition and a molecular evaporation setup for the growth of porphyrin thin films in a controlled environment (i.e., high vacuum). The system was tested against the fabrication of ZnTPP films on highly oriented pyrolytic graphite employing both techniques. Only electrospray deposition, where molecules are not sublimated but directly extracted from solution and sent to the substrate, was chosen for ZnPP molecules, given the presence of fragile side groups. *Ex situ* microscopic characterizations revealed, for the sprayed films, the presence of clusters producing a rough morphology, with differences depending on the molecular moiety. Evaporated films appear to be more uniform and flat; however, we found evidence of a regular arrangement of ZnTPP molecules in sprayed films, close to the HOPG surface. Finally, we demonstrated the possibility of *in situ* characterization by means of optical and electron spectroscopies of the molecular films produced via electrospray deposition. This makes the described apparatus particularly suited for the study of hybrid interfaces featuring a broad range of molecule/substrate combinations, including delicate molecular formulations and particularly reactive substrates.

ACKNOWLEDGMENTS

A.C. gratefully acknowledges the financial support from the European Union – Next Generation EU, PNRR - M4C2, investment 1.1, and Fondo PRIN 2022, within project ‘Functionalized Surfaces by True Molecular Bottom-Up Growth’ (FUTURO), Grant No. ID 2022FWZCHK, CUP D53D23009110006.

AUTHOR DECLARATIONS

Conflict of Interest

The authors have no conflicts to disclose.

Author Contributions

F. Goto: Data curation (lead); Investigation (lead); Writing – original draft (equal). **A. Calloni:** Methodology (equal); Project administration (equal); Writing – review & editing (equal). **R. Yivlialin:** Data curation (equal); Investigation (equal). **A. Bossi:** Investigation (equal); Writing – review & editing (equal). **F. Ciccacci:** Funding acquisition (equal); Writing – review & editing (equal). **L. Duò:** Resources (equal); Writing – review & editing (equal). **J. N. O’Shea:** Resources (equal); Validation (equal). **G. Bussetti:** Conceptualization (equal); Supervision (equal); Writing – review & editing (equal).

DATA AVAILABILITY

The data that support the findings of this study are available within the article.

REFERENCES

- R. Yivlialin, G. Bussetti, M. Penconi, A. Bossi, F. Ciccacci, M. Finazzi, and L. Duò, “Vacuum-deposited porphyrin protective films on graphite: Electrochemical atomic force microscopy investigation during anion intercalation,” *ACS Appl. Mater. Interfaces* **9**, 4100 (2017).
- M. A. Deyab and G. Mele, “Stainless steel bipolar plate coated with polyaniline/Zn-porphyrin composites coatings for proton exchange membrane fuel cell,” *Sci. Rep.* **10**, 3277 (2020).
- M. Penconi, R. Yivlialin, G. Bussetti, L. Duò, A. Bossi, and A. Orbelli Biroli, “Customised porphyrin coating films for graphite electrode protection: An investigation on the role of peripheral groups by coupled AFM and cyclic voltammetry techniques,” *Appl. Surf. Sci.* **507**, 145055 (2020).
- R. Paolesse, S. Nardis, D. Monti, M. Stefanelli, and C. Di Natale, “Porphyrinoids for chemical sensor applications,” *Chem. Rev.* **117**, 2517 (2017).
- G. Magna, M. Muduganti, M. Stefanelli, Y. Sivalingam, F. Zurlo, E. Di Bartolomeo, A. Catini, E. Martinelli, R. Paolesse, and C. Di Natale, “Light-activated porphyrinoid-capped nanoparticles for gas sensing,” *ACS Appl. Nano Mater.* **4**, 414 (2021).
- G. Bengasi, R. Meunier-Prest, K. Baba, A. Kumar, A. L. Pellegrino, N. D. Boscher, and M. Bouvet, “Molecular engineering of porphyrin-tapes/phthalocyanine heterojunctions for a highly sensitive ammonia sensor,” *Adv. Electr. Mater.* **6**, 2000812 (2020).
- K. Gao *et al.*, “Deep absorbing porphyrin small molecule for high-performance organic solar cells with very low energy losses,” *J. Am. Chem. Soc.* **137**, 7282 (2015).
- G. Bottari, G. de la Torre, D. M. Guldi, and T. Torres, “An exciting twenty-year journey exploring porphyrinoid-based photo- and electro-active systems,” *Coord. Chem. Rev.* **428**, 213605 (2021).
- T. Kim and K. Lee, “D- π -A conjugated molecules for optoelectronic applications,” *Macromol. Rapid Commun.* **36**, 943 (2015).
- M. Jurow, A. E. Schuckman, J. D. Batteas, and C. M. Drain, “Porphyrins as molecular electronic components of functional devices,” *Coord. Chem. Rev.* **254**, 2297 (2010).
- P. Zwick, D. Dulić, H. S. J. van der Zant, and M. Mayor, “Porphyrins as building blocks for single-molecule devices,” *Nanoscale* **13**, 15500 (2021).

- ¹²G. Magna, D. Monti, C. Di Natale, R. Paolesse, and M. Stefanelli, "The assembly of porphyrin systems in well-defined nanostructures: An update," *Molecules* **24**, 4307 (2019).
- ¹³L. Grill, M. Dyer, L. Lafferentz, M. Persson, M. V. Peters, and S. Hecht, "Nano-architectures by covalent assembly of molecular building blocks," *Nat. Nanotechnol.* **2**, 687 (2007).
- ¹⁴R. Yivlialin, M. Penconi, G. Bussetti, A. O. Biroli, M. Finazzi, L. Duò, and A. Bossi, "Morphological changes of porphine films on graphite by perchloric acid and phosphoric electrolytes," *Appl. Surf. Sci.* **442**, 501 (2018).
- ¹⁵J. M. Gottfried, "Surface chemistry of porphyrins and phthalocyanines," *Surf. Sci. Rep.* **70**, 259 (2015).
- ¹⁶G. Bussetti *et al.*, "Stable alignment of tautomers at room temperature in porphyrin 2D layers," *Adv. Funct. Mater.* **24**, 958 (2014).
- ¹⁷M. S. Jagadeesh, A. Calloni, A. Brambilla, A. Picone, A. Lodesani, L. Duò, F. Ciccacci, M. Finazzi, and G. Bussetti, "Room temperature magnetism of ordered porphyrin layers on Fe," *Appl. Phys. Lett.* **115**, 082404 (2019).
- ¹⁸T. Meng, P. Lei, and Q. Zeng, "Progress in the self-assembly of porphyrin derivatives on surfaces: STM reveals," *New J. Chem.* **45**, 15739 (2021).
- ¹⁹A. Orbelli Biroli *et al.*, "Out-of-plane metal coordination for a True solvent-free building with molecular bricks: Dodging the surface ligand effect for on-surface vacuum self-assembly," *Adv. Funct. Mater.* **31**, 2011008 (2021).
- ²⁰S. R. Forrest, "Ultrathin organic films grown by organic molecular beam deposition and related techniques," *Chem. Rev.* **97**, 1793 (1997).
- ²¹N. D. Boscher, G. Bengasi, and K. Heinze, "Chemical vapor deposition of porphyrins," in *Applications of Porphyrinoids as Functional Materials* (The Royal Society of Chemistry, 2021), pp. 121–148.
- ²²M. Tonezzer, A. Quaranta, G. Maggioni, S. Carturan, and G. D. Mea, "Optical sensing responses of tetraphenyl porphyrins toward alcohol vapours: A comparison between vacuum evaporated and spin-coated thin films," *Sens. Actuators, B* **122**, 620 (2007).
- ²³H. Suzuki, T. Yamada, T. Kamikado, Y. Okuno, and S. Mashiko, "Deposition of thermally unstable molecules with the spray-jet technique on Au(111) surface," *J. Phys. Chem B* **109**, 13296 (2005).
- ²⁴C. Guan, L. Li, D. Chen, Z. Gao, and W. Sun, "Thermal behavior and thermal decomposition study of porphyrin polymers containing different spacer groups," *Thermochim. Acta* **413**, 31 (2004).
- ²⁵G. J. Van Berkel, S. A. McLuckey, and G. L. Glush, "Electrospray ionization of porphyrins using a quadrupole ion trap for mass analysis," *Anal. Chem.* **63**, 1098 (1991).
- ²⁶J. C. Swarbrick, J. B. Taylor, and J. N. O'Shea, "Electrospray deposition in vacuum," *Appl. Surf. Sci.* **252**, 5622 (2006).
- ²⁷A. Saywell, G. Magnano, C. J. Satterley, L. M. A. Perdigão, N. R. Champness, P. H. Beton, and J. N. O'Shea, "Electrospray deposition of C60 on a hydrogen-bonded supramolecular network," *J. Phys. Chem. C* **112**, 7706 (2008).
- ²⁸L. C. Mayor, J. Ben Taylor, G. Magnano, A. Rienzo, C. J. Satterley, J. N. O'Shea, and J. Schnadt, "Photoemission, resonant photoemission, and x-ray absorption of a Ru(II) complex adsorbed on rutile TiO₂(110) prepared by *in situ* electrospray deposition," *J. Chem. Phys.* **129**, 114701 (2008).
- ²⁹A. Saywell, A. J. Britton, N. Taleb, M. del Carmen Giménez-López, N. R. Champness, P. H. Beton, and J. N. O'Shea, "Single molecule magnets on a gold surface: *In situ* electrospray deposition, x-ray absorption and photoemission," *Nanotechnology* **22**, 075704 (2011).
- ³⁰W. Richter and J.-T. Zettler, "Real-time analysis of III-V-semiconductor epitaxial growth," *Appl. Surf. Sci.* **100–101**, 465 (1996).
- ³¹W. G. Schmidt, P. H. Hahn, F. Bechstedt, N. Esser, P. Vogt, A. Wange, and W. Richter, "InP(001)-(2 × 1) surface: A hydrogen stabilized structure," *Phys. Rev. Lett.* **90**, 126101 (2003).
- ³²M. Zorn *et al.*, "Temperature dependence of the InP(001) bulk and surface dielectric function," *Appl. Phys. A: Mater. Sci. Process.* **65**, 333 (1997).
- ³³R. Passmann, P. Favero, W. G. Schmidt, R. Miotto, W. Braun, W. Richter, M. Kneissl, N. Esser, and P. Vogt, "Adsorption structure of cyclopentene on InP (001) (2 × 4)," *Phys. Rev. B* **80**, 125303 (2009).
- ³⁴G. Bussetti *et al.*, "Reflectance anisotropy spectroscopy: A probe to explore organic epitaxial growth," *J. Vac. Sci. Technol., A* **27**, 1029 (2009).
- ³⁵G. Ramanath, C. Rowe, G. Sharma, V. Venkataramani, J. G. Alauzun, R. Sundararaman, P. Koblinski, D. G. Sangiovanni, P. Eklund, and H. Pedersen, "Engineering inorganic interfaces using molecular nanolayers," *Appl. Phys. Lett.* **122**, 260502 (2023).
- ³⁶C. Rowe, S. Kumar Shanmugham, G. Greczynski, L. Hultman, A. le Febvrier, P. Eklund, and G. Ramanath, "Molecularly-induced roughness and oxidation in cobalt/organodithiol/cobalt nanolayers synthesized by sputter-deposition and molecular sublimation," *Dalton Trans.* **53**, 6451 (2024).
- ³⁷A. Rienzo, L. C. Mayor, G. Magnano, C. J. Satterley, E. Ataman, J. Schnadt, K. Schulte, and J. N. O'Shea, "X-ray absorption and photoemission spectroscopy of zinc protoporphyrin adsorbed on rutile TiO₂(110) prepared by *in situ* electrospray deposition," *J. Chem. Phys.* **132**, 084703 (2010).
- ³⁸R. González-Moreno *et al.*, "Following the metalation process of protoporphyrin IX with metal substrate atoms at room temperature," *J. Phys. Chem. C* **115**, 6849 (2011).
- ³⁹R. Yivlialin, L. Ferraro, C. Filoni, I. Majumdar, A. Calloni, F. Goto, M. Finazzi, L. Duò, F. Ciccacci, and G. Bussetti, "Probing the correlation between morphology and optical anisotropy in ZnTPP films grown at different temperatures," *Appl. Surf. Sci.* **611**, 155729 (2023).
- ⁴⁰G. Berti, A. Calloni, A. Brambilla, G. Bussetti, L. Duò, and F. Ciccacci, "Direct observation of spin-resolved full and empty electron states in ferromagnetic surfaces," *Rev. Sci. Instrum.* **85**, 073901 (2014).
- ⁴¹F. Ciccacci, E. Vescovo, G. Chiaia, S. De Rossi, and M. Tosca, "Spin-polarized electron gun for electron spectroscopies," *Rev. Sci. Instrum.* **63**, 3333 (1992).
- ⁴²Specific precautions have to be taken in order to avoid organic film damage or charging effects with intense electron beams, such as those employed in LEED and IPES.
- ⁴³Molecularspray Ltd. can provide an optional miniaturized heating system for the capillary region.
- ⁴⁴A first attempt of increasing the beam divergence through a simple electrostatic lens we placed downstream the final aperture of the ESD system proved not to be effective, possibly due to the presence of neutral species and/or too energetic molecular clusters in the beam.
- ⁴⁵C. Hamann, R. Woltmann, I. P. Hong, N. Hauptmann, S. Karan, and R. Berndt, "Ultrahigh vacuum deposition of organic molecules by electrospray ionization," *Rev. Sci. Instrum.* **82**, 033903 (2011).
- ⁴⁶G. Bussetti, L. Ferraro, A. Bossi, M. Campione, L. Duò, and F. Ciccacci, "A microprocessor-aided platform enabling surface differential reflectivity and reflectance anisotropy spectroscopy," *Eur. Phys. J. Plus* **136**, 421 (2021).
- ⁴⁷G. S. Marks, "The biosynthesis of heme and chlorophyll," *Bot. Rev.* **32**, 56 (1966).
- ⁴⁸R. H. Temperton, J. N. O'Shea, and D. J. Scurr, "On the suitability of high vacuum electrospray deposition for the fabrication of molecular electronic devices," *Chem. Phys. Lett.* **682**, 15 (2017).
- ⁴⁹R. Yivlialin, C. Filoni, F. Goto, A. Calloni, L. Duò, F. Ciccacci, and G. Bussetti, "Optical anisotropy of porphyrin nanocrystals modified by the electrochemical dissolution," *Molecules* **27**, 8010 (2022).
- ⁵⁰W. R. Scheidt, J. U. Mondal, C. W. Eigenbrot, A. Adler, L. J. Radonovich, and J. L. Hoard, "Crystal and molecular structure of the silver(II) and zinc(II) derivatives of meso-tetraphenylporphyrin. An exploration of crystal-packing effects on bond distance," *Inorg. Chem.* **25**, 795 (1986).
- ⁵¹S. Iannotta and T. Toccoli, "Supersonic molecular beam growth of thin films of organic materials: A novel approach to controlling the structure, morphology, and functional properties," *J. Polym. Sci., Part B: Polym. Phys.* **41**, 2501 (2003).
- ⁵²K. Walzer, T. Toccoli, A. Pallaoro, S. Iannotta, C. Wagner, T. Fritz, and K. Leo, "Comparison of organic thin films deposited by supersonic molecular-beam epitaxy and organic molecular-beam epitaxy: The case of titanil phthalocyanine," *Surf. Sci.* **600**, 2064 (2006).
- ⁵³Y. Wu, T. Toccoli, J. Zhang, N. Koch, E. Iacob, A. Pallaoro, S. Iannotta, and P. Rudolf, "Key role of molecular kinetic energy in early stages of pentacene island growth," *Appl. Phys. A* **95**, 21 (2009).
- ⁵⁴K. Tomita, N. Shioya, R. Kise, T. Shimoaka, H. Yoshida, T. Koganezawa, K. Eda, and T. Hasegawa, "Structure control of a zinc tetraphenylporphyrin thin film by vapor annealing using fluorine containing solvent," *Thin Solid Films* **665**, 85 (2018).

- ⁵⁵M. Ali, M. Abbas, S. K. Shah, E. Bontempi, A. Di Cicco, and R. Gunnella, "Film forming properties of electrosprayed organic heterojunctions," *Eur. Phys. J. Appl. Phys.* **62**, 30202 (2013).
- ⁵⁶M. Abbas, M. Ali, S. K. Shah, F. D'Amico, P. Postorino, S. Mangialardo, M. C. Guidi, A. Cricenti, and R. Gunnella, "Control of structural, electronic, and optical properties of eumelanin films by electrospray deposition," *J. Phys. Chem B* **115**, 11199 (2011).
- ⁵⁷G. Bussetti, S. Trabattini, S. Uttiya, A. Sassella, M. Riva, A. Picone, A. Brambilla, L. Duò, F. Ciccacci, and M. Finazzi, "Controlling drop-casting deposition of 2D Pt-octaethyl porphyrin layers on graphite," *Synth. Met.* **195**, 201 (2014).
- ⁵⁸N. C. M. Magdaong, M. Taniguchi, J. R. Diers, D. M. Niedzwiedzki, C. Kirmaier, J. S. Lindsey, D. F. Bocian, and D. Holten, "Photophysical properties and electronic structure of zinc(II) porphyrins bearing 0-4 meso-phenyl substituents: Zinc porphine to zinc tetraphenylporphyrin (ZnTPP)," *J. Phys. Chem. A* **124**, 7776 (2020).
- ⁵⁹C. Li and T. Imae, "Protoporphyrin IX zinc(II) organization at the air/water interface and its Langmuir-Blodgett films," *Langmuir* **19**, 779 (2003).
- ⁶⁰A. Picone *et al.*, "Local structure and morphological evolution of ZnTPP molecules grown on Fe(001)- $p(1 \times 1)$ O studied by STM and NEXAFS," *Appl. Surf. Sci.* **435**, 841 (2018).
- ⁶¹G. Bussetti, M. Campione, A. Sassella, and L. Duò, "Optical and morphological properties of ultra-thin H₂TPP, H₄TPP and ZnTPP films," *Phys. Status Solidi B* **252**, 100 (2015).
- ⁶²C. P. Ponce, H. Y. Araghi, N. K. Joshi, R. P. Steer, and M. F. Paige, "Spectroscopic and structural studies of a surface active porphyrin in solution and in Langmuir-Blodgett films," *Langmuir* **31**, 13590 (2015).
- ⁶³G. Bussetti, A. Calloni, M. Celeri, R. Yivlialin, M. Finazzi, F. Bottegoni, L. Duò, and F. Ciccacci, "Structure and electronic properties of Zn-tetra-phenylporphyrin single- and multi-layers films grown on Fe(001)- $p(1 \times 1)$ O," *Appl. Surf. Sci.* **390**, 856 (2016).
- ⁶⁴M. Franke, F. Marchini, H.-P. Steinrück, O. Lytken, and F. J. Williams, "Surface porphyrins metalate with Zn ions from solution," *J. Phys. Chem. Lett.* **6**, 4845 (2015).
- ⁶⁵R. Jöhr *et al.*, "Thermally induced anchoring of a zinc-carboxyphenylporphyrin on rutile TiO₂ (110)," *J. Chem. Phys.* **146**, 184704 (2017).
- ⁶⁶J. Spadavecchia, C. Méthivier, J. Landoulsi, and C. Pradier, "Interaction of ZnII Porphyrin with TiO₂ nanoparticles: From mechanism to synthesis of hybrid nanomaterials," *ChemPhysChem* **14**, 2462 (2013).
- ⁶⁷A. Siokou, F. Ravani, S. Karakalos, O. Frank, M. Kalbac, and C. Galiotis, "Surface refinement and electronic properties of graphene layers grown on copper substrate: An XPS, UPS and EELS study," *Appl. Surf. Sci.* **257**, 9785 (2011).
- ⁶⁸R. F. Willis, B. Feuerbacher, and B. Fitton, "Graphite conduction band states from secondary electron emission spectra," *Phys. Lett. A* **34**, 231 (1971).
- ⁶⁹G. Bussetti, A. Calloni, R. Yivlialin, A. Picone, F. Bottegoni, and M. Finazzi, "Filled and empty states of Zn-TPP films deposited on Fe(001)- $p(1 \times 1)$ O," *Beilstein J. Nanotechnol.* **7**, 1527 (2016).
- ⁷⁰S. Kitagawa, I. Morishima, T. Yonezawa, and N. Sato, "Photoelectron spectroscopic study on metalloctaethylporphyrins," *Inorg. Chem.* **18**, 1345 (1979).
- ⁷¹S. C. Khandelwal and J. L. Roebber, "The photoelectron spectra of tetraphenylporphine and some metallotetraphenylporphyrins," *Chem. Phys. Lett.* **34**, 355 (1975).
- ⁷²S. Rangan, S. Katalinic, R. Thorpe, R. A. Bartynski, J. Rochford, and E. Galoppini, "Energy level alignment of a zinc(II) tetraphenylporphyrin dye adsorbed onto TiO₂(110) and ZnO(1120) surfaces," *J. Phys. Chem. C* **114**, 1139 (2010).
- ⁷³A. Calloni *et al.*, "Cobalt atoms drive the anchoring of Co-TPP molecules to the oxygen-passivated Fe(001) surface," *Appl. Surf. Sci.* **505**, 144213 (2020).
- ⁷⁴L. Poggini *et al.*, "Electronic and magnetic properties of a monolayer of VOTPP molecules sublimated on Ag(100)," *Adv. Phys. Res.* **3**, 2300121 (2024).
- ⁷⁵D. M. Janas *et al.*, "Metalloporphyrins on oxygen-passivated iron: Conformation and order beyond the first layer," *Inorg. Chim. Acta* **557**, 121705 (2023).
- ⁷⁶In the case of molecular de-metalation, 2 out of 4 N atoms bind with protons. This results in a characteristic two-peak lineshape with XPS, as shown with ZnPP molecules on TiO₂ in Ref. 37, that, however, is not observed in the present case.
- ⁷⁷G. Albani, M. Capra, A. Lodesani, A. Calloni, G. Bussetti, M. Finazzi, F. Ciccacci, A. Brambilla, L. Duò, and A. Picone, "Self-assembly of C₆₀ on a ZnTPP/Fe(001)- $p(1 \times 1)$ O substrate: observation of a quasi-freestanding C₆₀ monolayer," *Beilstein J. Nanotechnol.* **13**, 857 (2022).
- ⁷⁸T. Aihara, S. A. Abd-Rahman, and H. Yoshida, "Metal screening effect on energy levels at metal/organic interface: Precise determination of screening energy using photoelectron and inverse-photoelectron spectroscopies," *Phys. Rev. B* **104**, 085305 (2021).
- ⁷⁹D. Yoshimura, H. Ishii, S. Narioka, M. Sei, T. Miyazaki, Y. Ouchi, S. Hasegawa, Y. Harima, K. Yamashita, and K. Seki, "The electronic structure of porphyrin/metal interfaces studied by UV photoemission spectroscopy," *Synth. Met.* **86**, 2399 (1997).
- ⁸⁰H. Yoshida, K. Yamada, J. Tsutsumi, and N. Sato, "Complete description of ionization energy and electron affinity in organic solids: Determining contributions from electronic polarization, energy band dispersion, and molecular orientation," *Phys. Rev. B* **92**, 075145 (2015).
- ⁸¹S. Kera and N. Ueno, "Photoelectron spectroscopy on the charge reorganization energy and small polaron binding energy of molecular film," *J. Electron Spectrosc. Relat. Phenom.* **204**, 2 (2015).
- ⁸²J. T. Dull *et al.*, "Thin-film organic heteroepitaxy," *Adv. Mater.* **35**, 2302871 (2023).